

## Research Paper

# Analytical spacecraft relative dynamics with gravitational, drag and third-body perturbations

Yazan Chihabi<sup>\*</sup>, Steve Ulrich

Department of Mechanical and Aerospace Engineering, Carleton University, Ottawa, Ontario, Canada

## ARTICLE INFO

## Keywords:

Spacecraft formation flying  
Spacecraft relative motion  
Spacecraft dynamics  
Analytical  
Orbital elements

## ABSTRACT

There has been a growing interest in spacecraft formation flying for space science applications. Such missions will require an accurate and efficient dynamics model, on-board the flight computer, to calculate and control the desired relative motion. Hence, an analytical dynamics model which can be applied to eccentric orbits and includes perturbations can provide an increase in accuracy and efficiency. This paper develops an accurate analytical solution of relative motion between two spacecraft using classical orbital elements. The analytical solution is obtained by propagating the orbital elements forward in time, while taking into account gravitational field up to the fifth harmonic, third-body and drag secular and periodic perturbations, and calculating the relative motion in the local-vertical–local-horizontal reference frame at each time-step. The analytical solution was observed to accurately describe the relative motion when compared with a numerical simulator, yielding errors on the order of meters for separation distances on the order of hundreds of meters.

## 1. Introduction

Space science missions, such as the mapping of other planets and moons, require the reduction of costs and an improvement of efficiency to meet the world's growing interest in space-related ventures [1]. Formation flying of multiple spacecraft is a key technology for such missions as it offers lower costs and increased efficiency by reducing the mass, power demand and size of the spacecraft buses. For example, European Space Agency's Proba-3 mission will use two spacecraft flying in formation in attempt to study the sun by creating an artificial solar eclipse [2]. However, formation flying has many considerations to be taken into account when compared to that of single spacecraft missions. The main considerations are with respect to the guidance system, since it is responsible for calculating the desired relative motion between the spacecraft. To ensure accuracy, the guidance system must take into account perturbations since ignoring orbital perturbations in the design of the reference trajectories would result in additional propellant consumption to force the follower spacecraft to follow the reference trajectory. Furthermore, the dynamics model must be accurate for high eccentricity values, and large separation distances while remaining computationally inexpensive for on-board implementation purposes. Accurate numerical models which take into account perturbations exist; however, they are computationally expensive and can lead to errors due to integration tolerances. Therefore, an analytical dynamics model is required since it satisfies these conditions and does not require numerical integration. Formulations which take into account perturbations,

such as the effects of gravitational field caused by oblateness of the earth, third body effects, and drag, can be found in literature. The gravitational perturbation is particularly significant when modeling orbits as it causes rotation of the line of apsides and precession of the line of nodes, along with changes in inclination and eccentricity values. The third body perturbation is also important when modeling higher altitude orbits since it also causes rotation of the line of apsides and precession of the line of nodes. Finally, drag is of concern when modeling low earth orbits (LEO) since drag acts in the opposite direction to the velocity vector and hence reduces the orbital energy which in turn reduces the orbital semi-major axis and eccentricity such that the spacecraft slowly spirals down.

The most used analytical model in formation flying is the Hill–Clohessy–Wiltshire (HCW) model [3], which provides linearized relative dynamics based upon exact non-linear differential equations of motion in the LVLH (local-vertical–local-horizontal) reference frame. The HCW model, due to the fact they are linearized equations of motion and time invariant, is adequate for the application of a linear state feedback controller design such as optimal feedback control method and linear quadratic regulator method. However, the model only works for circular Keplerian orbits as it does not take into account perturbations and simplifications made in the derivation causes it to be inaccurate for modeling elliptical reference orbits. When applying an eccentric reference orbit to the HCW model, the errors increase with

<sup>\*</sup> Corresponding author.

E-mail address: [Yazanchihabi@cmail.carleton.ca](mailto:Yazanchihabi@cmail.carleton.ca) (Y. Chihabi).

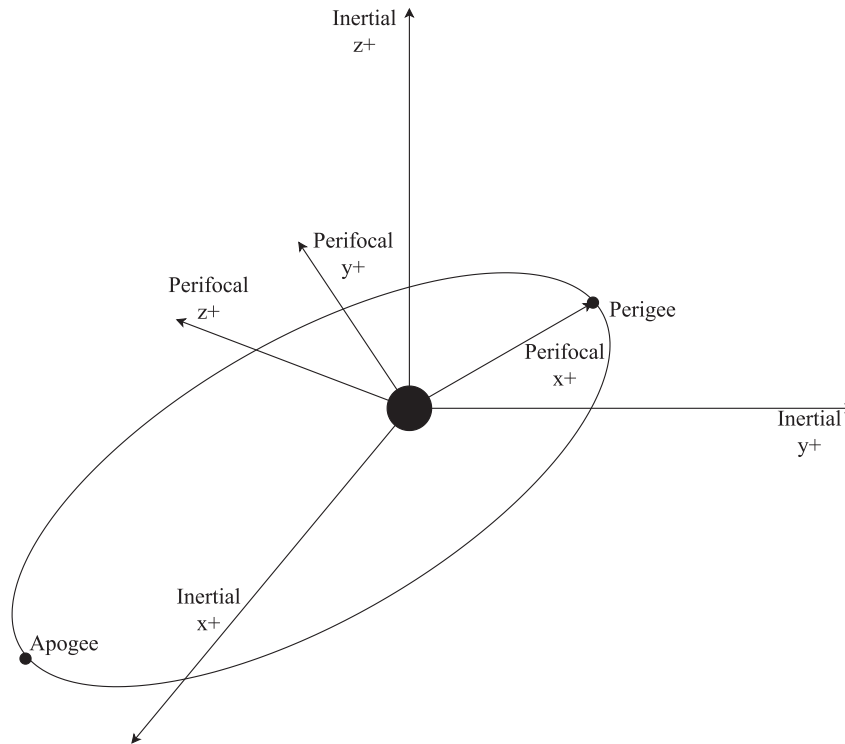


Fig. 1. Perifocal reference frame.

increasing eccentricity and it has been shown that the effect neglecting eccentricity in the HCW model greatly outweighs the effect of external perturbations [4]. Furthermore, the linear-time-invariant (LTI) HCW equations were extended by Inalhan, et al. [4] to include arbitrary eccentricity by reformulating the HCW as linear-parameter-varying (LPV) which enables the use of LPV control techniques, such as model predictive control. An analytical solution, which was first suggested by Hill [5] that incorporates Keplerian eccentric orbits and valid for any time-step, was formulated by Gurfil and Kholshevnikov [6,7]. The solution uses classical orbital elements as constant parameters to calculate the relative dynamics of a chaser spacecraft (analogous to a simple rotation matrix approach) instead of cartesian initial conditions used in the HCW model. The most important advantage of using this approach is the fact that the orbital elements can be made to vary as a function of time to include the effects of orbital perturbations [8,9]. Another analytical solution, proposed by Mahajan, et al. [10], uses linearized state transition matrices to propagate the relative mean orbital elements forward in time while taking into account the effects of gravitation field perturbation up to an arbitrary degree. Additionally, Guffanti et al. [11] developed state-transition matrix (STM) formulations using singular, quasi singular and non-singular orbital elements that included the singly averaged dynamical effects of  $J_2$ . The STM formulations were further developed to include doubly averaged third-body effects and solar radiation pressure [12]. Recently, Kuiack and Ulrich [13] developed a novel method in propagating relative motion analytically. Specifically, linearized short periodic and secular variations of the orbital elements formulated by Brouwer for the second zonal harmonic ( $J_2$ ) [14] were implemented into Gurfil and Kholshevnikov's equations of motion [6,7]. Using this formulation, Kuiack and Ulrich [13] implemented a back propagation technique such that a set of initial conditions for the chaser spacecraft in terms of orbital elements is found to allow the spacecraft to drift into a desired relative orbital elements.

The main contribution of this paper is extending the work by Kuiack and Ulrich [13] by including third body effects of the sun

and the moon, drag and gravitational perturbations up to the fifth harmonic. The third body perturbation linearized equations used were formulated by Prado [15,16] and Kozai [17,18] formulated linearized equations for effects of lunisolar perturbations on orbital elements, and Blitzer [19] formulated equations for drag. Furthermore, Brouwer [14], Liu [20], and Kozai [21] formulated equations for the gravitational perturbation up to fifth zonal harmonic ( $J_5$ ). This contrasts from Kuiack and Ulrich [13], where the authors had only implemented linearized short periodic and secular variations of the orbital elements formulated by Brouwer for the second zonal harmonic ( $J_2$ ) [14] into Gurfil and Kholshevnikov's equations of motion [6,7]. Therefore, by including the effects of additional perturbations, the work presented in this paper aims to improve the accuracy of the analytical model developed by Kuiack and Ulrich [13].

This paper is organized as follows: Section 2 describes the nonlinear equations of motion formulated by Gurfil and Kholshevnikov, and Section 3. describes the perturbing equations. Section 4 presents simulation results for the newly developed solution and concluding remarks are provided in Section 5.

## 2. Nonlinear analytical equations of relative motion

For completeness, this section presents the derivation of nonlinear analytical equations of relative motion formulated by Gurfil and Kholshevnikov [6,7].

### 2.1. Reference frames

A total of three reference frames are needed to derive equations of relative motion: the Earth-centered inertial (ECI), the perifocal and finally the local-vertical-local-horizon (LVLH) reference frames.

The ECI reference frame is denoted by  $\mathcal{F}_I$  and defined by its orthonormal unit vectors  $[\vec{I}_x, \vec{I}_y, \vec{I}_z]^T$  with its origin at the center of Earth.

The unit vector  $\vec{I}_z$  is aligned with the Earth's axis of rotation in the direction of the North Pole, and  $\vec{I}_x$  and  $\vec{I}_y$  lie on the Earth's equatorial plane. Furthermore,  $\vec{I}_x$  points in the direction of the vernal equinox with  $\vec{I}_y$  completing the triad such that the reference frame remains fixed in space and  $\vec{I}_y = \vec{I}_z \times \vec{I}_x$  (see Fig. 1).

The perifocal reference frame is denoted by  $F_p$  and defined by its orthonormal unit vectors  $[\vec{P}_x, \vec{P}_y, \vec{P}_z]^T$  with its origin also at the center of Earth. The unit vector  $\vec{P}_z$  points in the same direction as the orbit's angular momentum vector normal to the orbital plane,  $\vec{P}_x$  and  $\vec{P}_y$  lie on the orbital plane with  $\vec{P}_x$  pointing in the direction of the perigee, and  $\vec{P}_y$  completing the triad such that  $\vec{P}_y = \vec{P}_z \times \vec{P}_x$ . For the purposes of this paper, two perifocal reference frames are used and denoted as  $F_p^t$  and  $F_p^c$  for the target and chaser spacecraft respectively (see Fig. 2).

Finally, the LVLH reference frame is denoted by  $F_L$  and defined by its orthonormal unit vectors  $[\vec{L}_x, \vec{L}_y, \vec{L}_z]^T$  with its origin at the target spacecraft. The unit vector  $\vec{L}_z$  points in the same direction as the orbit's angular momentum vector normal to the orbital plane.  $\vec{L}_x$  points in the direction of the target's inertial position  $\vec{r}_t$  and  $\vec{L}_y$  completing the triad such that  $\vec{L}_y = \vec{L}_z \times \vec{L}_x$ .

### 2.2. Gurfil and Kholshchevnikov's equations of relative motion

The equations of motion formulated by Gurfil and Kholshchevnikov provides a method of calculating the relative motion of two spacecraft using each spacecraft's orbital elements [6,7]. Since this method uses orbital elements, the calculated relative motion remains accurate for any value of eccentricity.

First, the relative position vector of the chaser spacecraft with respect to the target, denoted as  $\vec{\rho}$ , is defined as

$$\vec{\rho} = \vec{r}_c - \vec{r}_t \tag{1}$$

where  $\vec{r}_c$  and  $\vec{r}_t$  respectively denote the position vectors of the chaser and target spacecraft. Expressed as components in the LVLH reference frame, Eq. (1) becomes

$$\rho_L = r_{cL} - r_{tL} \tag{2}$$

where  $r_{cL}$  and  $r_{tL}$  are the position vector components of the chaser and target spacecraft expressed in  $F_L$ .

To find the position vector components of the chaser spacecraft in the LVLH reference frame, two rotation matrices are required. The first rotation matrix converts the position vector components in  $F_p^c$  to  $F_I$  using  $C_{IP_c}(\omega_c, i_c, \Omega_c)$  defined as a 3-1-3 rotation sequence given by

$$C_{IP_c}(\omega_c, i_c, \Omega_c) = \begin{bmatrix} c_{\Omega_c} c_{\omega_c} - s_{\Omega_c} s_{\omega_c} c_{i_c} & -c_{\Omega_c} s_{\omega_c} - s_{\Omega_c} c_{\omega_c} c_{i_c} & s_{\Omega_c} s_{i_c} \\ s_{\Omega_c} c_{\omega_c} + c_{\Omega_c} s_{\omega_c} c_{i_c} & -s_{\Omega_c} s_{\omega_c} - c_{\Omega_c} c_{\omega_c} c_{i_c} & -c_{\Omega_c} s_{i_c} \\ s_{\omega_c} s_{i_c} & c_{\omega_c} s_{i_c} & c_{i_c} \end{bmatrix} \tag{3}$$

where  $\Omega_c$ ,  $i_c$  and  $\omega_c$  are the right ascension of the ascending node (RAAN), inclination, and argument of perigee of the chaser spacecraft, respectively. The second rotation matrix,  $C_{LI}$ , converts the position vector components of the chaser spacecraft in  $F_I$  to the  $F_p^t$  using  $C_{PI}(\omega_t, i_t, \Omega_t)$  given by

$$C_{PI}(\omega_t, i_t, \Omega_t) = \begin{bmatrix} c_{\Omega_t} c_{\omega_t} - s_{\Omega_t} s_{\omega_t} c_{i_t} & s_{\Omega_t} c_{\omega_t} + c_{\Omega_t} s_{\omega_t} c_{i_t} & s_{\omega_t} s_{i_t} \\ -c_{\Omega_t} s_{\omega_t} - s_{\Omega_t} c_{\omega_t} c_{i_t} & -s_{\Omega_t} s_{\omega_t} - c_{\Omega_t} c_{\omega_t} c_{i_t} & c_{\omega_t} s_{i_t} \\ s_{\Omega_t} s_{i_t} & -c_{\Omega_t} s_{i_t} & c_{i_t} \end{bmatrix} \tag{4}$$

and from  $F_p^t$  to  $F_L$  using  $C_{LP_t}(\theta_t)$  given by

$$C_{LP_t}(\theta_t) = \begin{bmatrix} c_{\theta_t} & s_{\theta_t} & 0 \\ -s_{\theta_t} & c_{\theta_t} & 0 \\ 0 & 0 & 1 \end{bmatrix} \tag{5}$$

such that Gurfil and Kholshchevnikov's equations of motion become

$$\rho_L = C_{LP_t}(\theta_t) C_{PI}(\omega_t, i_t, \Omega_t) C_{IP_c}(\omega_c, i_c, \Omega_c) r_{cP} - r_{tL} \tag{6}$$

where  $\theta_t$ ,  $\Omega_t$ ,  $i_t$  and  $\omega_t$  respectively denote the true anomaly, RAAN, inclination and argument of perigee of the target spacecraft and  $r_{cP}$  denotes the position vector components of the chaser spacecraft in  $F_p^c$  given by

$$r_{cP} = [r_c \cos \theta_c \quad r_c \sin \theta_c \quad 0]^T \tag{7}$$

where  $\theta_c$  is the true anomaly of the chaser spacecraft and  $r_{tL}$  is given by

$$r_{tL} = [r_t \quad 0 \quad 0]^T \tag{8}$$

and  $r_t$  and  $r_c$  are calculated using the orbit equation

$$r_t = \frac{a_t(1 - e_t^2)}{1 + e_t \cos \theta_t} \tag{9}$$

$$r_c = \frac{a_c(1 - e_c^2)}{1 + e_c \cos \theta_c} \tag{10}$$

where  $a_t$  and  $e_t$ , and  $a_c$  and  $e_c$  denote the semi major axis and eccentricity of the target and chaser spacecraft respectively.

### 3. Linearized equations for perturbed osculating orbital elements

In the previous section, the equations developed by Gurfil and Kholshchevnikov [6,7] apply constant orbital elements to calculate the relative motion of two spacecraft. However, if the changes in orbital elements due to perturbations can be calculated at every time-step, then the equations in the previous section may be modified to calculate the corresponding relative motion between both spacecraft. Hence, linearized equations that map the effects of perturbations to the orbital elements can be used. This section presents the linearized equations for the third body, gravitational and drag perturbations which will then be used in the following equations

$$a = \bar{a}_0 + \dot{\bar{a}}t + \Delta a_{lp} + \Delta a_{sp} \tag{11}$$

$$e = \bar{e}_0 + \dot{\bar{e}}t + \Delta e_{lp} + \Delta e_{sp} \tag{12}$$

$$i = \bar{i}_0 + \dot{\bar{i}}t + \Delta i_{lp} + \Delta i_{sp} \tag{13}$$

$$\omega = \bar{\omega}_0 + \dot{\bar{\omega}}t + \Delta \omega_{lp} + \Delta \omega_{sp} \tag{14}$$

$$\Omega = \bar{\Omega}_0 + \dot{\bar{\Omega}}t + \Delta \Omega_{lp} + \Delta \Omega_{sp} \tag{15}$$

$$M = \bar{M}_0 + \dot{\bar{M}}t + \Delta M_{lp} + \Delta M_{sp} \tag{16}$$

where  $[\bar{a}_0, \bar{e}_0, \bar{i}_0, \bar{\omega}_0, \bar{\Omega}_0, \bar{M}_0]^T$  denote the initial mean orbital elements,  $[\Delta a_{lp}, \Delta e_{lp}, \Delta i_{lp}, \Delta \omega_{lp}, \Delta \Omega_{lp}, \Delta M_{lp}]^T$  and  $[\Delta a_{sp}, \Delta e_{sp}, \Delta i_{sp}, \Delta \omega_{sp}, \Delta \Omega_{sp}, \Delta M_{sp}]^T$  denote the long and short periodic variations of orbital elements, and  $t$  is the time elapsed since  $t_0$ . In this paper, only gravitational long and short periodic effects are included. The terms  $[\dot{\bar{a}}, \dot{\bar{e}}, \dot{\bar{i}}, \dot{\bar{\omega}}, \dot{\bar{\Omega}}, \dot{\bar{M}}]^T$  denote the secular variations of orbital elements and given by

$$\dot{\bar{a}} = \dot{\bar{a}}_{3rd} + \dot{\bar{a}}_{drag} + \dot{\bar{a}}_{grav} \tag{17}$$

$$\dot{\bar{e}} = \dot{\bar{e}}_{3rd} + \dot{\bar{e}}_{drag} + \dot{\bar{e}}_{grav} \tag{18}$$

$$\dot{\bar{i}} = \dot{\bar{i}}_{3rd} + \dot{\bar{i}}_{drag} + \dot{\bar{i}}_{grav} \tag{19}$$

$$\dot{\bar{\omega}} = \dot{\bar{\omega}}_{3rd} + \dot{\bar{\omega}}_{drag} + \dot{\bar{\omega}}_{grav} \tag{20}$$

$$\dot{\bar{\Omega}} = \dot{\bar{\Omega}}_{3rd} + \dot{\bar{\Omega}}_{drag} + \dot{\bar{\Omega}}_{grav} \tag{21}$$

$$\dot{\bar{M}} = \dot{\bar{M}}_{3rd} + \dot{\bar{M}}_{drag} + \dot{\bar{M}}_{grav} \tag{22}$$

where the subscripts '3rd', 'drag', and 'grav' denote the contributions of third body, drag and gravitational up to the fifth zonal harmonic.

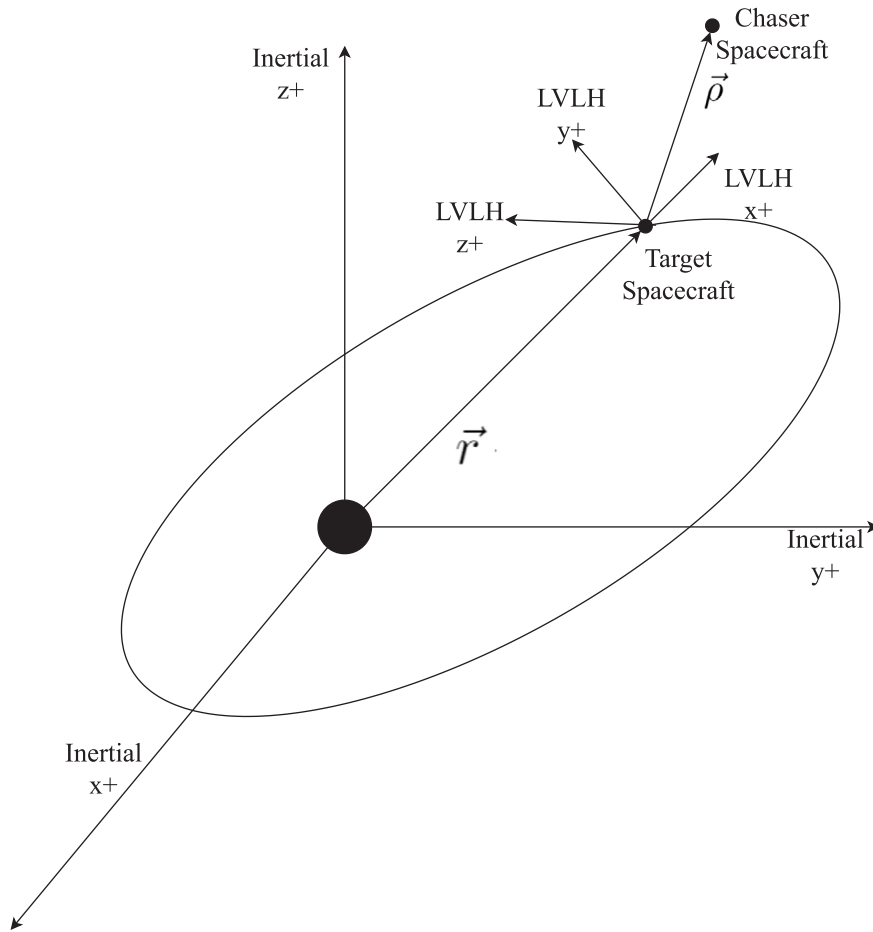


Fig. 2. Local-vertical–local-horizontal reference frame.

### 3.1. Third body model

The effects of third body perturbations on satellite orbits have been studied extensively in the past and continue to be an active research area. Kozai [18] developed the first secular and long-periodic equations on the effects of luni-solar perturbations on a satellite’s orbital elements based on the assumption that the distance of the satellite from the Earth was very small compared to the moon and that the moon’s orbit is circular. Those equations were re-visited by him to include short periodic terms [17]. Smith [22] extended Kozai’s theory to include secular changes for a third body in an elliptical orbit and found that for NASA’s Echo 1 mission, the perigee radius decreased as much as 100 meters over 25 days.<sup>1</sup> The finding demonstrates the importance of including the third body perturbation when planning trajectories for highly elliptical orbits. Vallado [23, p. 636–641] also concluded that third body perturbation causes secular variations about RAAN and argument of perigee with small effects on mean anomaly, and causes periodic variations with the eccentricity, inclination, RAAN, and argument of perigee. Furthermore, Vallado [23, p. 604–612] also concluded that third body mainly affects high altitude orbits, whereas gravitational and drag dominate low altitudes and LEO. Luni-solar effects on orbital elements were also developed by Cook [24] who also included the effects of solar radiation pressure, Kaula [25] and Giacaglia [26] who also developed secular and periodic variations.

Furthermore, Musen, et al. [27] expanded on Kozai’s theory where they observed that the third body perturbation causes the perigee height of a satellite to increase with periodic variations over long durations (20 km increase over approximately one month duration) due to third body effects on eccentricity. Recently, Domingos, et al. [16] and Prado [15], developed a simplified analytical model for a satellite’s orbital elements based on the third body disturbing function expanded in Legendre polynomials up to fourth order. Specifically, the developed analytical model double averaged the expanded disturbing function over the satellite’s orbital period and then again over the third body’s. This work uses Prado’s double averaged model [16] expanded to the second order for the case of an elliptical third body. Here, these equations will be used in terms of mean values which are provided by

$$\dot{a}_{3rd} = 0 \tag{23}$$

$$\dot{e}_{3rd} = \frac{15Kn^2 \bar{e} \sqrt{1 - \bar{e}^2}}{8\bar{n}} \left[ 1 + 1.5e'^2 + \frac{15}{8}e'^4 \right] \sin^2 \bar{i} \sin 2\bar{\omega} \tag{24}$$

$$\dot{i}_{3rd} = -\frac{15Kn^2 \bar{e}^2}{16\bar{n} \sqrt{1 - \bar{e}^2}} \left[ 1 + 1.5e'^2 + \frac{15}{8} \right] \sin 2\bar{i} \sin 2\bar{\omega} \tag{25}$$

$$\begin{aligned} \dot{\omega}_{3rd} = & \frac{3Kn^2}{8\bar{n} \sqrt{1 - \bar{e}^2}} \left[ 1 + 1.5e'^2 + \frac{15}{8}e'^4 \right] \left[ (5 \cos^2 \bar{i} - 1 + \bar{e}^2) \right. \\ & \left. + 5(1 - \bar{e}^2 - \cos^2 \bar{i}) \cos 2\bar{\omega} \right] \end{aligned} \tag{26}$$

$$\dot{\Omega}_{3rd} = \frac{3Kn^2 \cos \bar{i}}{8\bar{n} \sqrt{1 - \bar{e}^2}} \left[ 1 + 1.5e'^2 + \frac{15}{8}e'^4 \right] [5\bar{e}^2 \cos 2\bar{\omega} - 3\bar{e}^2 - 2] \tag{27}$$

<sup>1</sup> <https://history.nasa.gov/SP-4308/ch6.htm>.

$$\dot{M}_{3rd} = -\frac{Kn^2}{8\bar{n}} \left[ 1 + 1.5e'^2 + \frac{15}{8}e'^4 \right] [(3\bar{e}^2 + 7)(3\cos^2 \bar{i} - 1) + 15(1 + \bar{e}^2)\sin^2 \bar{i}\cos^2 \bar{\omega}] \quad (28)$$

where  $\bar{i}$ ,  $\bar{e}$ ,  $\bar{\omega}$ , and  $\bar{n}$  are the mean inclination, eccentricity, argument of perigee, and orbital motion of the satellite and where  $K$  and  $n'$  are given by

$$K = \frac{m'}{m' + m_0} \quad (29)$$

$$n' = \sqrt{\frac{\mu'}{a'^3}} \quad (30)$$

where  $K$  is the mass ratio of the third body with respect to orbiting body, in this case the Earth,  $m'$  is the mass of the third body,  $m_0$  is the mass of the central body, and  $n'$ ,  $e'$ , and  $a'$  are the mean orbital motion, eccentricity and semi-major axis of the third body, respectively.

These equations provide the changes in orbital elements due to a third body for general orbital elements. Roscoe et al. [28] expanded on Prado's model to provide a transformation for third body averaged model to osculating elements. This was done because the third body averaged model produces inaccurate results whenever long durations (1000s of days) and larger time-steps are used, due to the effect of discrepancies in initial conditions. However, since smaller time-steps (on the order of seconds) and shorter durations (on the order of 10 orbits) are required, the equations developed by Prado used in this paper are sufficient to model third body effects on spacecraft formations.

### 3.2. Drag model

Although atmospheric drag is extensively studied, an exact or accurate model is yet to exist. One of the main reasons is the fact that density is difficult to model mainly due to the effects of solar wind activity on the atmosphere. However, analytical approximations of the effects of drag on orbital elements exist in literature based on the exponential model for density. The first analytical model was formulated by Izsak [29] where the effects were separated in terms of periodic and secular variations. Izsak concluded that the greatest effects of drag are on the semi-major axis, eccentricity, argument of perigee and mean anomaly for which all undergo periodic variations and the semi-major axis, eccentricity and mean anomaly undergo secular variations. Xu, et al. [30] and Watson, et al. [31] also developed an analytical solution for drag, while Danielson [32] developed a semi-analytic solution and Martinusi et al. [33] developed a first order accurate analytical solution.

This paper focuses on the work of Lawden [19] who developed secular solutions for drag based on the exponential atmospheric model. These solutions will herein be used in terms of mean orbital elements and are provided as

$$\ddot{a}_{drag} = -\bar{n}\delta\bar{a}^2\rho[B_0 + 2\bar{e}B_1 + 0.75\bar{e}^2(B_0 + B_2) + 0.25(\bar{e}^3)(3B_1 + B_3)]\exp(-c), \quad (31)$$

$$\ddot{e}_{drag} = -\bar{n}\delta\bar{a}\rho[B_1 + 0.5\bar{e}(B_0 + B_2) - 0.125\bar{e}^2(5B_1 + B_3) - \frac{1}{16}\bar{e}^3(5B_0 + 4B_2 - B_4)]\exp(-c), \quad (32)$$

$$\dot{a}_{drag} = -\frac{0.25\bar{a}\omega_E\delta\rho}{\sqrt{Q}}\sin(\bar{i})[B_0 - 2\bar{e}B_1 + (B_2 - 2\bar{e}B_1)\cos(2\bar{\omega})]\exp(-c) \quad (33)$$

$$\dot{e}_{drag} = \frac{0.25\bar{a}\omega_E\delta\rho}{\sqrt{Q}}(B_2 - 2\bar{e}B_1)\sin(2\bar{\omega})\exp(-c) \quad (34)$$

$$\dot{\omega}_{drag} = -\dot{\bar{L}}_{drag}\cos(\bar{i}) \quad (35)$$

$$\dot{M}_{drag} = 0 \quad (36)$$

where  $\bar{n}$ ,  $\bar{e}$ ,  $\bar{a}$ , and  $\bar{\omega}$  are the mean orbital motion, eccentricity, semi-major axis and argument of perigee of a spacecraft respectively and  $\omega_E$  is angular velocity of Earth. The density at the perigee  $\rho$ , modified

Bessel function of the first kind  $B_j$  with argument  $c$  and the constants  $c$ ,  $Q$  and  $\delta$  are given by

$$\rho = \rho_0 \exp\left(-\frac{h_p - h_0}{H}\right) \quad (37)$$

$$h_p = \bar{a}(1 - \bar{e}) - R_E \quad (38)$$

$$B_j(c) = \left(\frac{c}{2}\right)^j \sum_{k=0}^{\infty} \frac{\left(\frac{c}{2}\right)^{2k}}{k!\Gamma(j+k+1)} \quad (39)$$

$$c = \frac{\bar{a}\bar{e}}{H} \quad (40)$$

$$Q = 1 - \frac{2\omega_E(1 - \bar{e})^{1.5}}{\bar{n}\sqrt{1 + \bar{e}}}\cos(\bar{i}) \quad (41)$$

$$\delta = \frac{QAC_D}{m} \quad (42)$$

where  $\rho_0$  is the atmospheric density in  $\text{kg/m}^3$  and  $H$  is the scale height at a reference altitude  $h_0$ ,  $h_p$  is altitude of perigee,  $Q$  is the factor for rotation of Earth's atmosphere (between 0.9–1.1),  $A$  is exposed area in  $\text{m}^2$  to the direction of fluid flow and  $C_D$  is the coefficient of drag and  $m$  is mass of the spacecraft in kg. It should be noted when using these equations for drag,  $\rho$  must be multiplied by a factor of 1000 since the units for distance and speed are in km and km/s for spacecraft applications.

### 3.3. Gravitational model

Finally, the last linearized model in this paper is the gravitational perturbation up to the fifth zonal harmonic. Recently, Kuiack and Ulrich [13] developed a model which only includes the second zonal harmonic in terms of its secular and short periodic variations based off of Brouwer's [14] gravitational equations. Vinti [34] expanded on Brouwer's [14] and Kozai's [21] work to include the effects of the residual fourth zonal harmonic. In addition, an analytical relative dynamics for a  $J_2$  perturbed elliptical orbit was formulated by Hamel and Lafontaine [35] but only included secular variations of RAAN, argument of perigee and mean anomaly. Liu [20] expanded on Brouwer's and Kozai's work to include secular variations of eccentricity and inclination, and concluded that their effects are small (about 0.5% more accurate). This paper combines the secular equations reformulated by Liu [20], and periodic equations formulated by Brouwer [14] and Kozai [18] with the secular solutions given by

$$\dot{a}_{grav} = 0 \quad (43)$$

$$\dot{e}_{grav} = -\frac{3}{32}\bar{n}J_2^2\left(\frac{R_E}{\bar{p}}\right)^4\sin^2(\bar{i})[14 - 15\sin^2(\bar{i})]\bar{e}(1 - \bar{e}^2)\sin(2\bar{\omega}) - \frac{3}{8}\bar{n}J_3\left(\frac{R_E}{\bar{p}}\right)^3\sin(\bar{i})[4 - 5\sin^2(\bar{i})](1 - \bar{e}^2)\cos(\bar{\omega}) \quad (44)$$

$$- \frac{15}{32}\bar{n}J_4\left(\frac{R_E}{\bar{p}}\right)^4\sin^2(\bar{i})[6 - 7\sin^2(\bar{i})]\bar{e}(1 - \bar{e}^2)\sin(2\bar{\omega})$$

$$\dot{i}_{grav} = \frac{3}{64}\bar{n}J_2^2\left(\frac{R_E}{\bar{p}}\right)^4\sin(2\bar{i})[14 - 15\sin^2(\bar{i})]\bar{e}^2\sin(2\bar{\omega}) + \frac{3}{8}\bar{n}J_3\left(\frac{R_E}{\bar{p}}\right)^3\cos(\bar{i})[4 - 5\sin^2(\bar{i})]\bar{e}\cos(\bar{\omega}) \quad (45)$$

$$+ \frac{15}{64}\bar{n}J_4\left(\frac{R_E}{\bar{p}}\right)^4\sin(2\bar{i})[6 - 7\sin^2(\bar{i})]\bar{e}^2\sin(2\bar{\omega})$$

$$\begin{aligned} \dot{\omega}_{grav} = & \frac{3}{4} \bar{n} J_2 \left( \frac{R_E}{\bar{p}} \right)^2 [4 - 5 \sin^2(\bar{i})] \\ & + \frac{9}{384} \bar{n} J_2^2 \frac{R_E^4}{\bar{p}^4} [56\bar{e}^2 + (760 - 36\bar{e}^2) \sin^2(\bar{i}) \\ & - (890 + 45\bar{e}^2) \sin^4(\bar{i})] - \frac{15}{128} \bar{n} J_4 \frac{R_E^4}{\bar{p}^4} [64 + 72\bar{e}^2 \\ & - (248 + 252\bar{e}^2) \sin^2 \bar{i} + (196 + 189\bar{e}^2) \sin^4(\bar{i})] \end{aligned} \tag{46}$$

$$\begin{aligned} \dot{\Omega}_{grav} = & -\frac{3J_2 R_E^2 \bar{n} \cos \bar{i}}{2\bar{p}^2} + \frac{3J_2^2 R_E^4 \bar{n} \cos \bar{i}}{32\bar{p}^4} [12 - 4\bar{e}^2 - (80 + 5\bar{e}^2) \sin^2(\bar{i})] \\ & + \frac{15J_4 R_E^4 \bar{n} \cos \bar{i}}{32\bar{p}^4} [8 + 12\bar{e}^2 - (14 + 21\bar{e}^2) \sin^2(\bar{i})] \end{aligned} \tag{47}$$

$$\begin{aligned} \dot{M}_{grav} = & \bar{n} + \frac{3\bar{n} J_2 R_E^2 \sqrt{1 - \bar{e}^2}}{4\bar{p}^2} [2 - 3 \sin^2(\bar{i})] \\ & + \frac{3\bar{n} J_2^2 R_E^4}{512\bar{p}^4 \sqrt{1 - \bar{e}^2}} [320\bar{e}^2 - 280\bar{e}^4 + (1600 - 1568\bar{e}^2 + 328\bar{e}^4) \sin^2(\bar{i}) \\ & + (-2096 + 1072\bar{e}^2 + 79\bar{e}^4) \sin^4(\bar{i})] \\ & - \frac{45\bar{n} J_4 R_E^4 \bar{e}^2 \sqrt{1 - \bar{e}^2}}{128\bar{p}^4} [-8 + 40 \sin(\bar{i}) - 35 \sin^2(\bar{i})] \end{aligned} \tag{48}$$

where  $J_2$  and  $J_4$  are the second and fourth zonal harmonics respectively,  $R_E$  is the mean radius of the Earth, and  $\bar{p}$  and  $\bar{n}$  are the semi-latus rectum and mean orbital motion of the satellite given by

$$\bar{p} = \bar{a}(1 - \bar{e}^2) \tag{49}$$

$$\bar{n} = \sqrt{\frac{\mu}{\bar{a}^3}} \tag{50}$$

and where  $\bar{a}$  and  $\bar{e}$  are the mean semi-major axis and eccentricity, respectively and  $\mu$  is the gravitational constant of the Earth.

The long periodic solutions are given by

$$\Delta a_{lp} = 0 \tag{51}$$

$$\begin{aligned} \Delta e_{lp} = & \left\{ \frac{1}{8} \lambda'_2 e(1 - e^2) [1 - 11 \cos^2(i) - 40 \cos^4(i)[1 - 5 \cos^2(i)]^{-1}] \right. \\ & - \left. \frac{5}{12} \frac{\lambda'_4}{\lambda'_2} e(1 - e^2)[1 - 3 \cos^2(i) - 8 \cos^4(i)[1 - 5 \cos^2(i)]^{-1}] \right\} \cos(2\omega) \\ & + \left\{ \frac{1}{4} \frac{\lambda'_3}{\lambda'_2} (1 - e^2) \sin(i) + \frac{5}{64} \frac{\lambda'_5}{\lambda'_2 (1 - e^2)} \sin(i)(4 + 3e^2) \times \right. \\ & + [1 - 9 \cos^2(i) - 24 \cos^4(i)[1 - 5 \cos^2(i)]^{-1}] \left. \right\} \sin(\omega) \\ & - \frac{35}{384} \frac{\lambda'_5}{\lambda'_2} e^2 (1 - e^2) \sin(i) \times \\ & [1 - 5 \cos^2(i) - 16 \cos^4(i)[1 - 5 \cos^2(i)]^{-1}] \sin(3\omega) \end{aligned} \tag{52}$$

$$\Delta i_{lp} = -\frac{e \Delta e_{lp}}{(1 - e)^2 \tan(i)} \tag{53}$$

$$\begin{aligned} \Delta \omega_{lp} = & \left\{ -\frac{1}{16} \lambda'_2 [(2 + e^2) - 11(2 + 3e^2) \cos^2(i)] \right. \\ & - 40(2 + 5e^2) \cos(i)^4 [1 - 5 \cos^2(i)]^{-1} - 400e^2 \cos^6(i)[1 - 5 \cos^2(i)]^{-2} \\ & + \frac{5}{24} \frac{\lambda'_4}{\lambda'_2} [(2 + e^2) - 3(2 + 3e^2) \cos^2(i)] \\ & - 8(2 + 5e^2) \cos(i)^4 [1 - 5 \cos^2(i)]^{-1} \\ & - 80e^2 \cos^6(i)[1 - 5 \cos^2(i)]^{-2} \left. \right\} \sin(2\omega) \\ & + \left\{ \frac{1}{4} \frac{\lambda'_3}{\lambda'_2} \left[ \frac{\sin i}{e} - \frac{e \cos^2(i)}{\sin(i)} \right] \right. \\ & + \frac{5}{64} \frac{\lambda'_5}{\lambda'_2} \left[ \left( \frac{1 - e^2}{e} \right) \frac{\sin i}{e} - \frac{e \cos^2(i)}{\sin(i)} \right] (4 + 3e^2) + e \sin(i)(26 + 9e^2) \\ & \times [1 - 9 \cos^2(i) - 24 \cos^4(i)[1 - 5 \cos^2(i)]^{-1}] \\ & - \frac{15}{32} \frac{\lambda'_5}{\lambda'_2} e \cos^2(i) \sin(i)(4 + 3e^2) \\ & \times [3 + 16 \cos^2(i)[1 - 5 \cos^2(i)]^{-1} + 40 \cos^4(i)(1 - 5 \cos^2(i))^{-2}] \left. \right\} \cos(\omega) \\ & + \left\{ -\frac{35}{1152} \frac{\lambda'_5}{\lambda'_2} [e \sin(i)(3 + 2e^2) \right. \\ & - \left. \frac{e^3 \cos^2(i)}{\sin(i)}] [1 - 5 \cos^2(i) - 16 \cos^4(i)[1 - 5 \cos^2(i)]^{-1}] \right. \\ & + \frac{35}{576} \frac{\lambda'_5}{\lambda'_2} e^3 \cos^2(i) \sin(i) \\ & \times [5 + 32 \cos^2(i)[1 - 5 \cos^2(i)]^{-1} \\ & \left. + 80 \cos^4(i)[1 - 5 \cos^2(i)]^{-2}] \right\} \cos(3\omega) \end{aligned} \tag{54}$$

$$\begin{aligned} \Delta \Omega_{lp} = & \left\{ -\frac{1}{8} \lambda'_2 e^2 \cos(i) [11 + 80 \cos(i)^2 [1 - 5 \cos^2(i)]^{-1}] \right. \\ & + 200 \cos^4(i) [1 - 5 \cos^2(i)]^{-2} + \frac{5}{12} \frac{\lambda'_4}{\lambda'_2} e^2 \cos(i) \times \\ & \left. \left[ 3 + 16 \cos(i)^2 [1 - 5 \cos^2(i)]^{-1} \right. \right. \\ & \left. \left. + 40 \cos^4(i) [1 - 5 \cos^2(i)]^{-2} \right] \right\} \sin(2\omega) \\ & + \left\{ \frac{1}{4} \frac{\lambda'_3}{\lambda'_2} \frac{e \cos(i)}{\sin(i)} + \frac{5}{64} \frac{\lambda'_5}{\lambda'_2} \frac{e \cos(i)}{\sin(i)} (4 + 3e^2) \right. \\ & \left. [1 - 9 \cos^2(i) - 24 \cos^4(i) [1 - 5 \cos^2(i)]^{-1}] \right. \\ & + \frac{15}{32} \frac{\lambda'_5}{\lambda'_2} e \cos(i) \sin(i)(4 + 3e^2) \\ & \times [3 + 16 \cos^2(i)[1 - 5 \cos^2(i)]^{-1} \\ & + 40 \cos^4(i)(1 - 5 \cos^2(i))^{-2}] \left. \right\} \cos(\omega) \\ & + \left\{ -\frac{35}{1152} \frac{\lambda'_5}{\lambda'_2} \frac{e^3 \cos(i)}{\sin(i)} [1 - 5 \cos^2(i) - 16 \cos^4(i) [1 - 5 \cos^2(i)]^{-1}] \right. \\ & - \frac{35}{576} \frac{\lambda'_5}{\lambda'_2} e^3 \cos(i) \sin(i) \\ & \times [5 + 32 \cos^2(i) [1 - 5 \cos^2(i)]^{-1} \\ & \left. + 80 \cos^4(i) [1 - 5 \cos^2(i)]^{-2}] \right\} \cos(3\omega) \end{aligned} \tag{55}$$

$$\begin{aligned} \Delta M_{1p} = & \left\{ \frac{1}{8} \lambda'_2 e (1 - e^2)^{\frac{3}{2}} [1 - 11 \cos^2(i) - 40 \cos^4(i) [1 - 5 \cos^2(i)]^{-1}] \right. \\ & \left. - \frac{5}{12} \frac{\lambda'_4}{\lambda'_2} (1 - e^2)^{\frac{3}{2}} [1 - 3 \cos^2(i) - 8 \cos^4(i) [1 - 5 \cos^2(i)]^{-1}] \right\} \sin(2\omega) \\ & + \left\{ -\frac{1}{4} \frac{\lambda'_3}{\lambda'_2} \frac{(1 - e^2)^{\frac{3}{2}}}{e} \sin(i) - \frac{5}{64} \frac{\lambda'_5}{\lambda'_2} \frac{(1 - e^2)^{\frac{3}{2}}}{e} \sin(i) (4 + 9e^2) \times \right. \\ & [1 - 9 \cos^2(i) - 24 \cos^4(i) [1 - 5 \cos^2(i)]^{-1}] \cos(\omega) \\ & + \frac{35}{384} \frac{\lambda'_5}{\lambda'_2} e (1 - e^2)^{\frac{3}{2}} \sin(i) \times \\ & \left. [1 - 5 \cos^2(i) - 16 \cos^4(i) [1 - 5 \cos^2(i)]^{-1}] \cos(3\omega) \right\} \end{aligned} \quad (56)$$

where  $\lambda'_2, \lambda'_3, \lambda'_4$ , and  $\lambda'_5$  are given by

$$\lambda'_2 = \frac{J_2 R_E^2}{2a^2(1 - e^2)^2} \quad (57)$$

$$\lambda'_3 = \frac{-J_3 R_E^3}{a^3(1 - e^2)^3} \quad (58)$$

$$\lambda'_4 = \frac{-3J_4 R_E^4}{8a^4(1 - e^2)^4} \quad (59)$$

$$\lambda'_5 = \frac{J_5 R_E^5}{a^5(1 - e^2)^5} \quad (60)$$

Finally, the short periodic variations are calculated as follows

$$\begin{aligned} \Delta a_{sp} = & \frac{J_2 R_E^2}{a} \left\{ \left( \frac{a}{r} \right)^3 - \frac{1}{(1 - e^2)^{3/2}} \right. \\ & \left. + \left[ -\left( \frac{a}{r} \right)^3 + \frac{1}{(1 - e^2)^{3/2}} + \left( \frac{a}{r} \right)^3 \cos(2\omega + 2\theta) \right] \frac{3 \sin^2(i)}{2} \right\} \end{aligned} \quad (61)$$

$$\begin{aligned} \Delta e_{sp} = & \frac{J_2 R_E^2}{4} \left\{ \frac{-2}{a^2 e \sqrt{1 - e^2}} + \frac{2a(1 - e^2)}{er^3} + \left[ \frac{3}{a^2 e \sqrt{1 - e^2}} - \frac{3a(1 - e^2)}{er^3} \right. \right. \\ & - \frac{3(1 - e^2) \cos(\theta + 2\omega)}{p^2} - \frac{3 \cos(2\theta + 2\omega)}{a^2 e (1 - e^2)} + \frac{3a(1 - e^2) \cos(2\theta + 2\omega)}{er^3} \\ & \left. \left. - \frac{(1 - e^2) \cos(3\theta + 2\omega)}{p^2} \right] \sin^2(i) \right\} \end{aligned} \quad (62)$$

$$\Delta i_{sp} = \frac{J_2 R_E^2 \sin(2i)}{8p^2} [3 \cos(2\omega + 2\theta) + 3e \cos(2\omega + \theta) + e \cos(2\omega + 3\theta)] \quad (63)$$

$$\begin{aligned} \Delta \Omega_{sp} = & \frac{J_2 R_E^2 \cos(2i)}{4p^2} [6(\theta - M + e \sin \theta) - 3 \sin(2\omega + 2\theta) \\ & - 3e \cos(2\omega + \theta) - e \cos(2\omega + 3\theta)] \end{aligned} \quad (64)$$

$$\begin{aligned} \Delta \omega_{sp} = & \frac{3J_2 R_E^2}{2p^2} \left\{ \left( 2 - \frac{5}{2} \sin^2 i \right) (\theta - M + e \sin \theta) \right. \\ & + \left( 1 - \frac{3}{2} \sin^2 i \right) \left[ \frac{1}{e} \left( 1 - \frac{e^2}{4} \right) \sin \theta + \frac{1}{2} \sin(2\theta) + \frac{e}{12} \sin(3\theta) \right] \\ & - \frac{1}{e} \left[ \frac{1}{4} \sin^2 i + \left( \frac{1}{2} - \frac{15}{16} \sin^2 i \right) e^2 \right] \sin(\theta + 2\omega) \\ & + \frac{e}{16} \sin^2(i) \sin(\theta - 2\omega) \\ & - \frac{1}{2} \left( 1 - \frac{5}{2} \sin^2 i \right) \sin(2\theta + 2\omega) \\ & + \frac{1}{e} \left[ \frac{7}{12} \sin^2 i - \frac{1}{6} \left( 1 - \frac{19}{8} \sin^2 i \right) e^2 \right] \times \\ & \left. \sin(3\theta + 2\theta) + \frac{3}{8} \sin^2 i \sin(4\theta + 2\omega) + \frac{e}{16} \sin^2 i \sin(5\theta + 2\omega) \right\} \end{aligned} \quad (65)$$

$$\begin{aligned} \Delta M_{sp} = & \frac{3J_2 R_E^2 \sqrt{1 - e^2}}{2ep^2} \left\{ -\left( 1 - \frac{3}{2} \sin^2 i \right) \times \right. \\ & \left[ \left( 1 - \frac{e^2}{4} \right) \sin \theta + \frac{e}{2} \sin(2\theta) + \frac{e^2}{12} \sin(3\theta) \right] + \sin^2 i \left[ \frac{1}{4} \left( 1 + \frac{5}{4} e^2 \right) \times \right. \\ & \sin(\theta + 2\omega) - \frac{e^2}{16} \sin(\theta - 2\omega) - \frac{7}{12} \left( 1 - \frac{e^2}{28} \right) \sin(3\theta + 2\theta) \\ & \left. \left. - \frac{3e}{8} \sin(4\theta + 2\omega) - \frac{e^2}{16} \sin(5\theta + 2\omega) \right] \right\} \end{aligned} \quad (66)$$

Since the short periodic variations are functions of the true anomaly,  $\theta$ , a way of computing it is required. Gurfil and Kholshvnikov [6] proposed to numerically integrate for the time derivative of the true anomaly. However, the purpose of this paper is to provide a fully analytical solution. Many solutions to obtain the true anomaly from the mean anomaly, eccentric anomaly and the orbit's eccentricity exist in literature. Vallado [23, p. 80–81] illustrates many of these methods, including a method that uses modified Bessel functions of the first kind paired with the eccentricity and mean anomaly to solve for the true anomaly. Kuiuack and Ulrich [13] provided a simple analytical approximation for the true anomaly in terms of the eccentric anomaly. The simple recursive solution is given by

$$E = M + e \sin(M + e \sin(M + e \sin(M + \dots + e \sin(M)))) \quad (67)$$

$$\cos \theta = \frac{\cos E - e}{1 - e \cos E} \quad (68)$$

$$\sin \theta = \frac{\sqrt{1 - e^2} \sin E}{1 - e \cos E} \quad (69)$$

$$\theta = \tan^{-1} \frac{\sin \theta}{\cos \theta} \quad (70)$$

where  $E$  is the eccentric anomaly. This is a recursive solution based on the Newton–Raphson Iteration Technique<sup>2</sup> which implies an infinite series. Therefore, the expression will become truncated based on the desired accuracy.

### 3.4. Procedure to obtain relative motion solution

This section presents the procedure, summarized in steps, to obtain the relative motion solution by using the perturbed equations presented in the previous sections.

1. Two sets of Keplerian osculating orbital elements are first initialized:  $[a_{c_0}, e_{c_0}, i_{c_0}, \omega_{c_0}, \Omega_{c_0}, \theta_{c_0}]^T$  and  $[a_{t_0}, e_{t_0}, i_{t_0}, \omega_{t_0}, \Omega_{t_0}, \theta_{t_0}]^T$ .
2. The mean anomaly of each spacecraft,  $M_{c_0}$  and  $M_{t_0}$ , are then initialized by using Eqs. (67)–(70) and the true anomalies of each spacecraft.
3. The initial osculating orbital elements and mean anomalies are used with Eqs. (51)–(66) to calculate long and short periodic variations due to gravitational field perturbation.
4. Equations (11)–(16) are then rearranged to solve for the initial mean orbital elements for both spacecraft, i.e

$$\begin{aligned} \bar{a}_0 &= a_0 - \Delta a_{0p} - \Delta a_{0sp} \\ \bar{e}_0 &= e_0 - \Delta e_{0p} - \Delta e_{0sp} \\ \bar{i}_0 &= i_0 - \Delta i_{0p} - \Delta i_{0sp} \\ \bar{\omega}_0 &= \omega_0 - \Delta \omega_{0p} - \Delta \omega_{0sp} \\ \bar{\Omega}_0 &= \Omega_0 - \Delta \Omega_{0p} - \Delta \Omega_{0sp} \\ \bar{M}_0 &= M_0 - \Delta M_{0p} - \Delta M_{0sp} \end{aligned}$$

<sup>2</sup> [http://web.mit.edu/10.001/Web/Course\\_Notes/NLAE/node6.html](http://web.mit.edu/10.001/Web/Course_Notes/NLAE/node6.html).

5. The mean orbital motion and mean semi-latus rectum for each spacecraft,  $\bar{n}_c$ ,  $\bar{p}_c$ ,  $\bar{n}_t$ , and  $\bar{p}_t$ , are calculated using Eqs. (49) and (50).
6. The mean orbital elements  $[\dot{a}_c, \dot{e}_c, \dot{i}_c, \dot{\omega}_c, \dot{\Omega}_c, \dot{M}_c]^T$  and  $[\dot{a}_t, \dot{e}_t, \dot{i}_t, \dot{\omega}_t, \dot{\Omega}_t, \dot{M}_t]^T$  can now be propagated using the initial mean values from the previous step and Eqs. (23)–(48). The accuracy of the solution can further be improved by re-calculating the mean rates at every time-step.
7. The long and short periodic variations for every time-step are then calculated using Eqs. (51)–(66) and mean orbital elements calculated in step 6. The periodic variations are then added with the mean orbital elements to obtain the osculating orbital elements at each time-step.
8. Using propagated osculating mean anomalies, the osculating true anomalies are also propagated using Eqs. (67)–(70).
9. The orbit radii of each spacecraft,  $r_c$  and  $r_t$ , can then be calculated using Eqs. (9) and (10).
10. Finally, the relative motion in LVLH is calculated using Eq. (6) with Eqs. (3)–(5), and (7)–(8) evaluated with the perturbed osculating orbital elements.

#### 4. Numerical simulations

This section presents a comparison of results obtained using the equations developed in this paper against a numerical propagator that integrates the exact nonlinear differential equations of motion in  $\mathcal{F}_I$  to verify the accuracy of the model. Specifically, effects of adding perturbations to the analytical model were compared for LEO and HEO formations. Furthermore, the full analytical model is applied to the Proba-3 mission and is compared against the numerical propagator, and a sensitivity analysis of the model is performed by varying eccentricity and formation size.

The numerical propagator used in all simulation results presented here integrates the inertial two-body equation of motion to which the exact inertial perturbing accelerations are added. Specifically, perturbing accelerations due to gravitational field through the expansion of gravitational potential function up to degree and order 180 [36], the exact third body effects of the sun, moon and solar system planets through using the inertial coordinates provided by JPL Planetary Ephemeris, ocean and solid Earth tidal effects, relativity [36], solar radiation pressure, and drag were calculated [23] then converted from inertial to LVLH reference frame. The solver used for the numerical propagator for all cases was selected as a ODE45 with a relative and absolute tolerance of  $1 \times 10^{-9}$ . For the drag model, it is assumed that both spacecraft maximum surface area is always perpendicular to the flow direction and that the atmosphere rotates with the Earth, and constant coefficient of drag for both spacecraft of 2.3 is used. The mass and surface area are 211 kg and 1.77 m<sup>2</sup>, and 339 kg and 3.34 m<sup>2</sup> for the chaser and target spacecraft, respectively [2]. For the solar radiation pressure model, a constant surface area equal assumed to be the same as the drag model (i.e: a spherical spacecraft) with a coefficient of reflectivity of 2. These values are used for all cases presented.

For the proposed analytical solution's third body model only the effects of the sun and the moon were considered. The Earth was assumed to be in a circular orbit around the sun and moon's eccentricity is constant at 0.0536. The Solar and Lunar data were provided by NASA's Jet Propulsion Laboratory Horizons website based off measurements made on July 1, 2018.<sup>3</sup> In addition, the analytical model ignores the orbit inclination, RAAN and argument of perigee of the sun and the moon.

The osculating orbital elements for the LEO example are initialized as  $a = 7106.14$  km,  $i = 98.3^\circ$ ,  $\omega = 0^\circ$ ,  $\Omega = 270^\circ$ , and  $\theta = 0^\circ$  for both

spacecraft, whereas  $e_t = 0.05$  and  $e_c = 0.05 + 0.001$  [13]. Fig. 3 shows the results obtained by both the full analytical model and numerical propagator for the initial conditions over 10 orbits. The relative position error is defined as the difference, in the LVLH reference frame, between the analytical model and numerical propagator. The full analytical model produces bounded errors for the radial and in-track directions, whereas the error increases with time in the along-track direction. Figs. 4–6 show results of the analytical model after the effects of third body, drag, and gravitational short and long periodic variations were removed from the analytical model. Fig. 5 shows the errors that is obtained when Kuiack and Ulrich's [13] analytical model was compared against the numerical propagator. Specifically, Fig. 6 shows that removing the effects of long and short periodic variations cause a drastic increase in errors about all three axes and becomes unbounded.

Figs. 7–10 show the results of removing perturbations from both the numerical propagator and the analytical model. Fig. 7 shows the results assuming a Keplerian orbit, while Fig. 9 shows the effects of J2–J5 gravitational perturbation model and Fig. 10 shows luni-solar third-body and drag effects. The errors obtained for the Keplerian case is a result of the numerical integration tolerances, which can be observed when comparing Figs. 7 and 8. The errors in Fig. 9 emphasize that the analytical model considering the gravitational perturbations produces bounded errors. Fig. 10 shows that although the analytical equations for drag and third-body accurately predicts the relative motion, the solution in the along-track direction diverges with time.

For the HEO case, the osculating orbital elements are initialized as  $a = 36944$  km,  $i = 59.0^\circ$ ,  $\omega = 188^\circ$ ,  $\Omega = 84.0^\circ$ , and  $\theta = 0^\circ$  for both spacecraft, whereas  $e_t = 0.811$  and  $e_c = e_t + (5 \times 10^{-5})$  for the target and chaser spacecraft respectively [2]. This initialization is an estimated representation of the Proba-3 case. Fig. 11 shows the full analytical model while Figs. 12–15 show the results of omitting third body, drag and gravitational periodic effects. Specifically, Fig. 14 shows the errors that is obtained when Kuiack and Ulrich's [13] analytical model was compared against the numerical propagator. The error growth increased slightly when third body and drag effects were removed from the analytical model, with drag having the larger contribution. This is due to the fact that, at the perigee, the spacecraft encounter higher drag forces as a result of the high velocity. Error growth increased dramatically when the periodic variations due to gravitational field were omitted.

Figs. 16–18 show results for formation sizes between 100 and 80 000 meters by varying the chaser eccentricity of the Proba-3 case using the full analytical model. Specifically, the errors in Figs. 16–17 were shown to be significantly large for short relative distances which is likely due to the perturbations not taken into account within the analytical model. In terms of Fig. 18, errors for the first three orbits remained relatively small for all three directions and attained a maximum error of 1200 meters for a separation distance of 80 000 meters in the along-track direction. Furthermore, it was observed that accuracy increases as the initial separation in eccentricity increases. This implies that, if initial conditions for each spacecraft were carefully selected, the model would provide more accurate results. Fig. 19 shows the results for a combined in-plane and out-of-plane initialization using separations in eccentricity and inclinations for a target initialized with the same orbital elements as Proba-3. On the other hand, Fig. 20 shows the results for separations in all six classical orbital elements. By comparing Figs. 19–20 with Fig. 18, the analytical solution maintains accuracy in all three directions of relative motion while showing bounded errors.

Figs. 21–23 show results obtained by the full analytical model by varying Proba-3 target eccentricity values between 0.01 and 0.6. By comparison with Fig. 20, it was observed that errors increase significantly with increasing eccentricity, and error spikes start to appear beyond an eccentricity of 0.6. The time rate of change of true anomaly,  $\dot{\theta}$ , is inversely proportional to spacecraft's position,  $r$ , and is given by

$$\dot{\theta} = \frac{h}{r^2} \quad (71)$$

<sup>3</sup> <https://ssd.jpl.nasa.gov/horizons.cgi>.

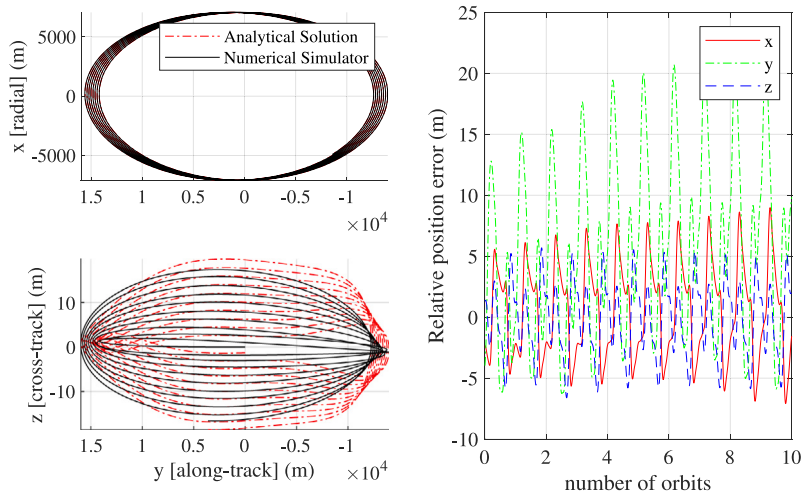


Fig. 3. LEO full analytical model.

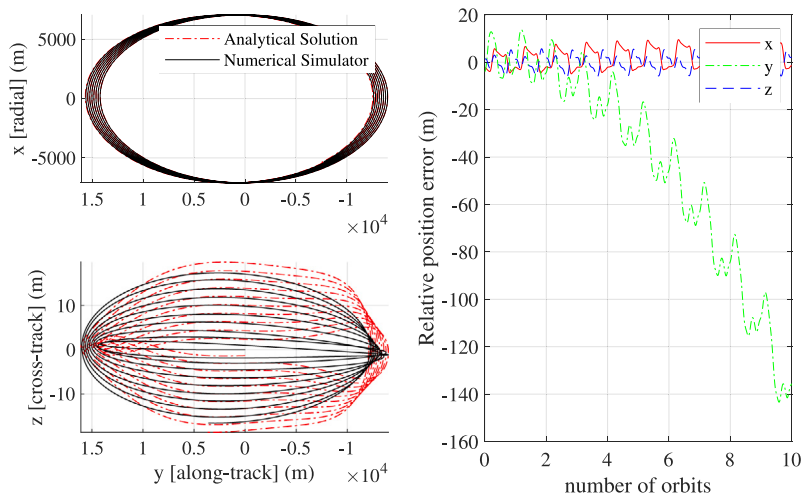


Fig. 4. LEO analytical model: Third body = 0 and drag = 0.

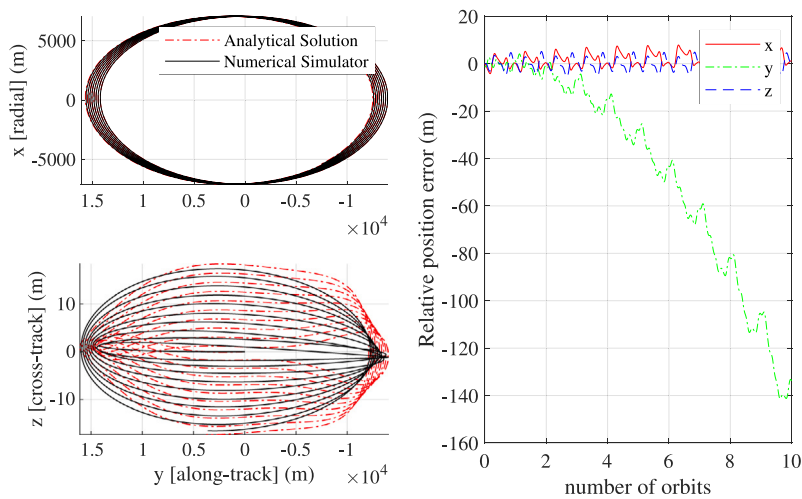


Fig. 5. LEO analytical model: Third body = 0, drag = 0 and gravitational long periodic variations = 0.

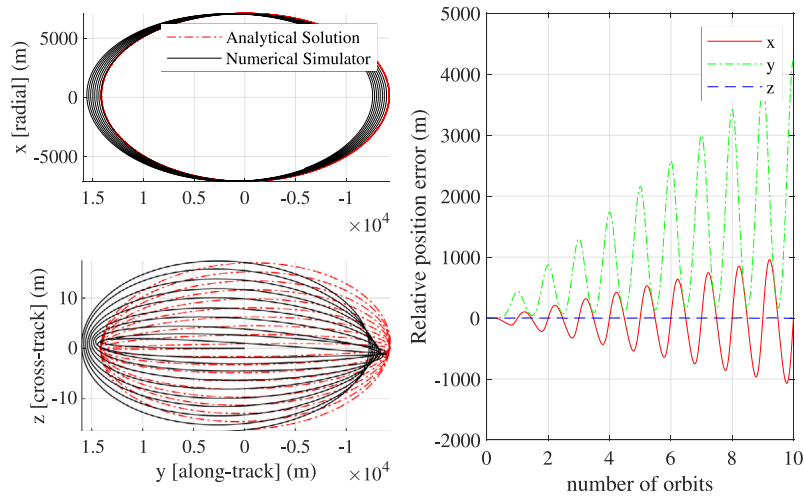


Fig. 6. LEO analytical model: Third body = 0, drag = 0 and gravitational short & long periodic variations = 0.

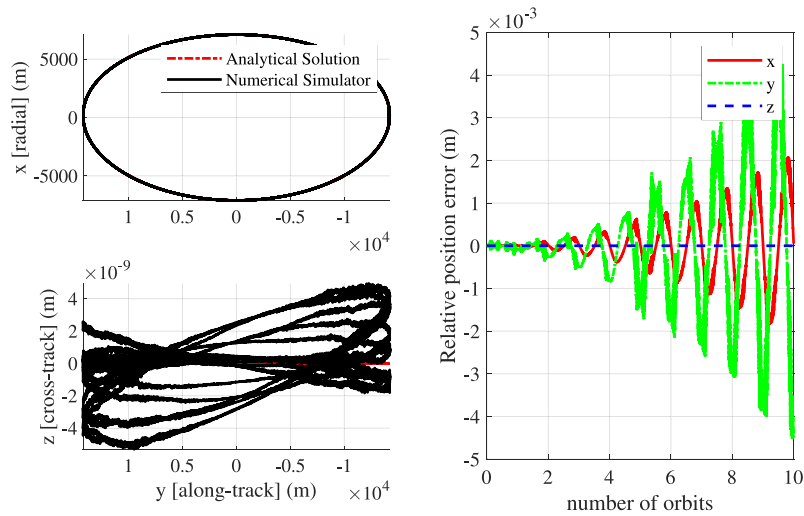


Fig. 7. LEO analytical & numerical model: Two-body.

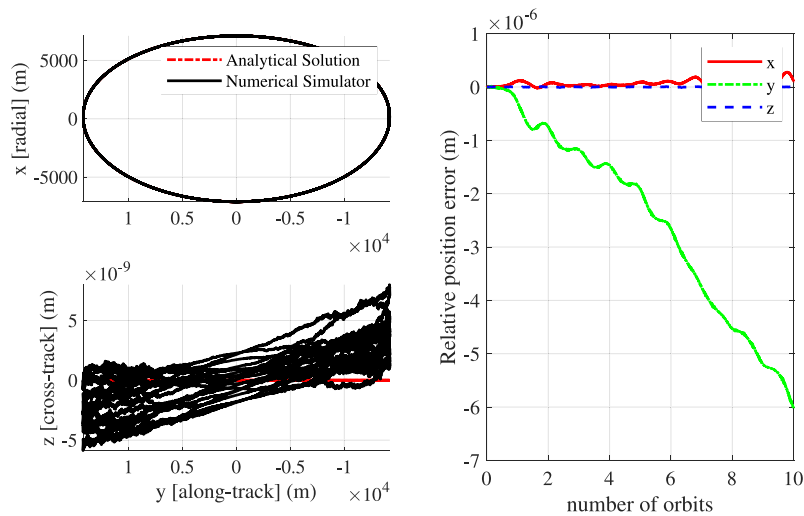


Fig. 8. LEO analytical & numerical model (relative tolerance  $1 \times 10^{-14}$ ): Two-body.

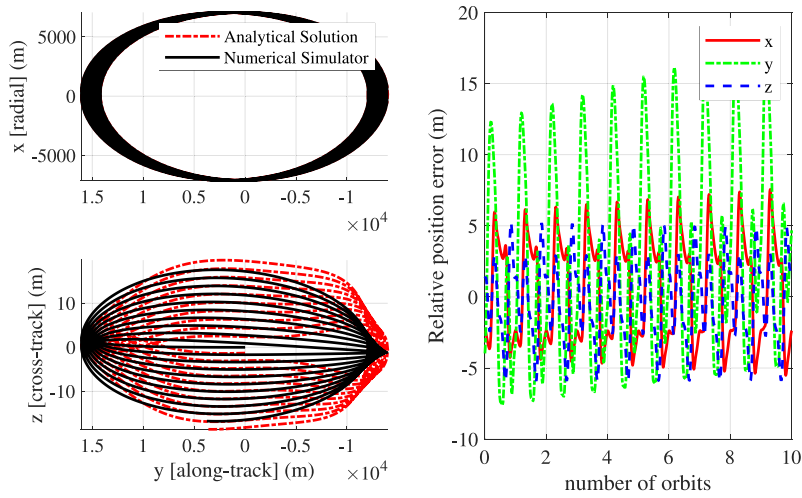


Fig. 9. LEO analytical & numerical model: J2-J5.

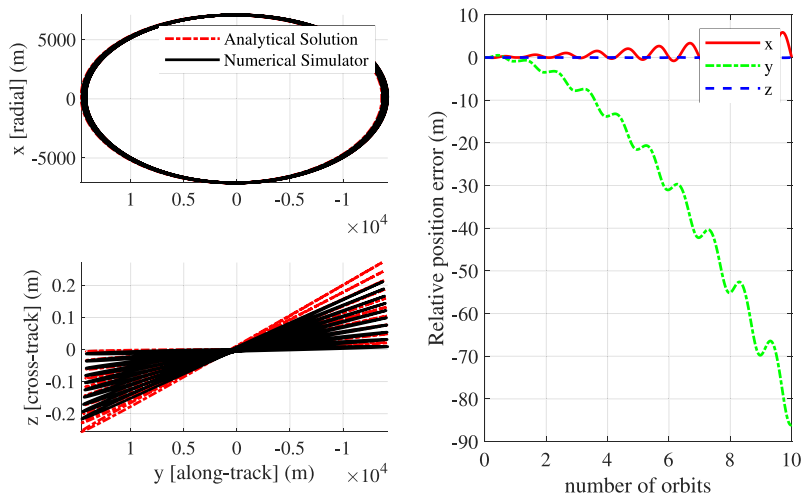


Fig. 10. LEO analytical & numerical model: Third-body and drag.

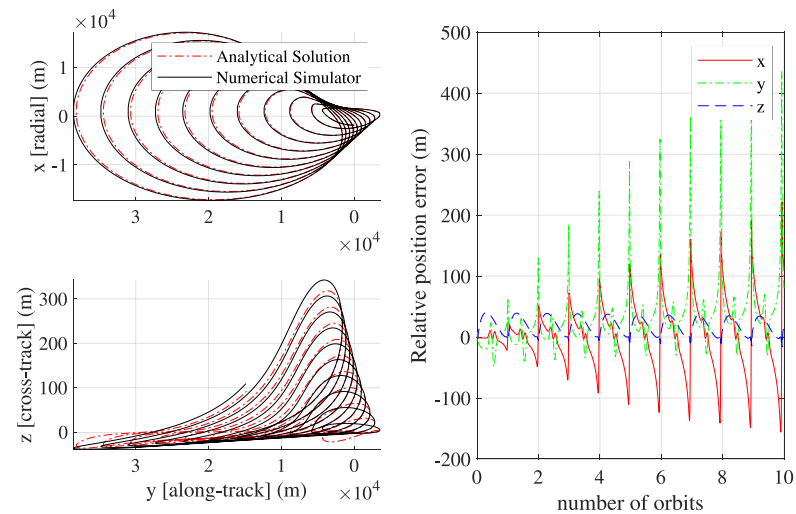


Fig. 11. PROBA-3 full analytical model.

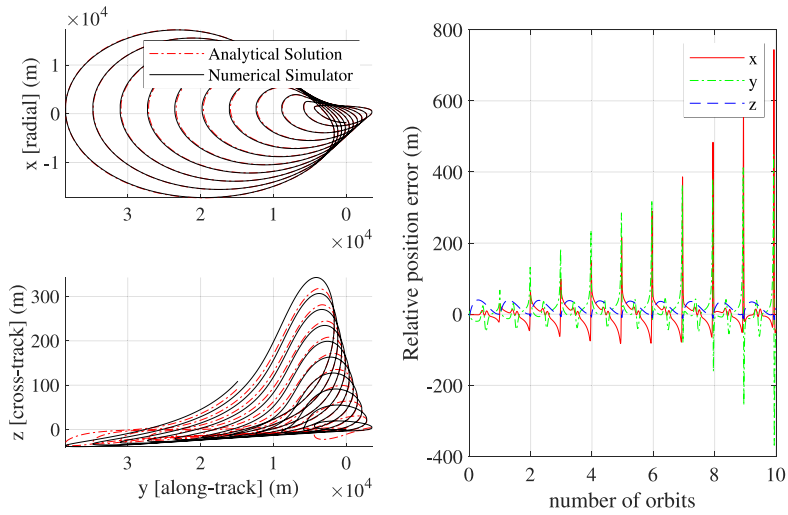


Fig. 12. PROBA-3 analytical model: Third body = 0.

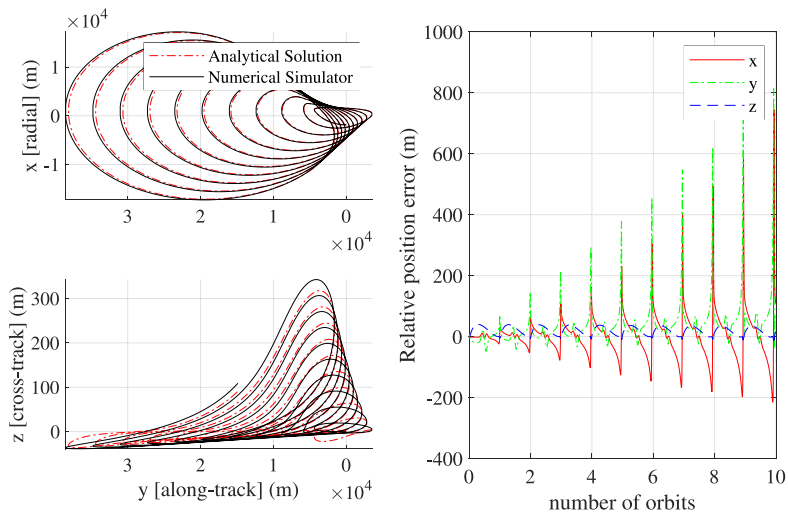


Fig. 13. PROBA-3 analytical model: Third body = 0 and drag = 0.

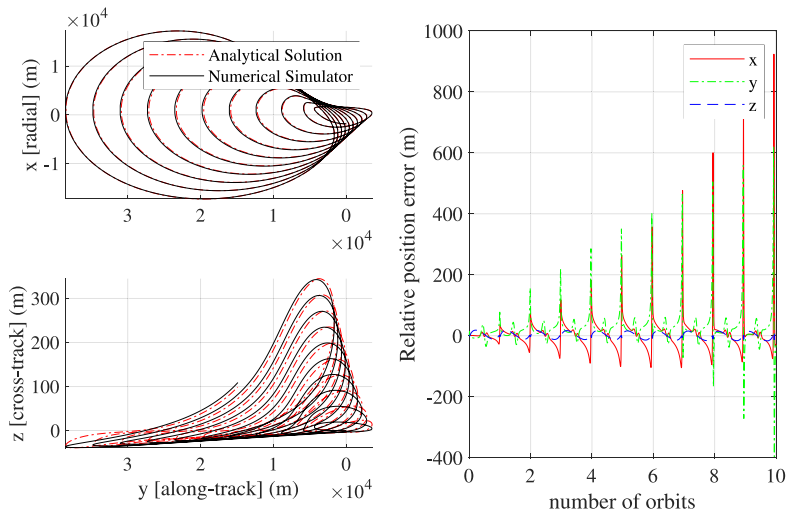


Fig. 14. PROBA-3 analytical model: Third body = 0, drag = 0 and gravitational long periodic variations = 0.

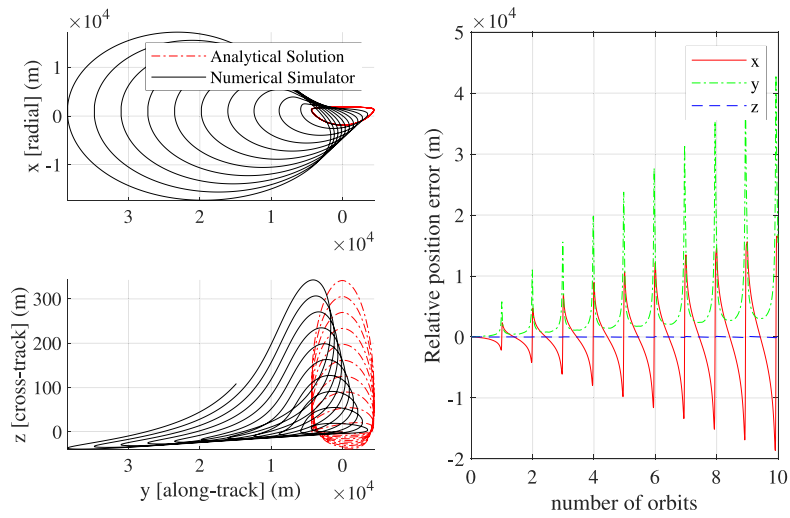


Fig. 15. PROBA-3 analytical model: Third body = 0, drag = 0 and gravitational short & long periodic variations = 0.

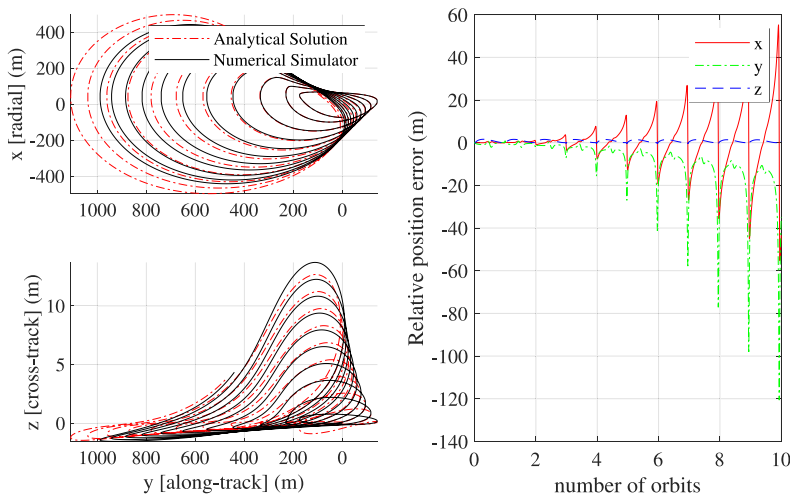


Fig. 16.  $e_c = e_t + 0.000002$ .

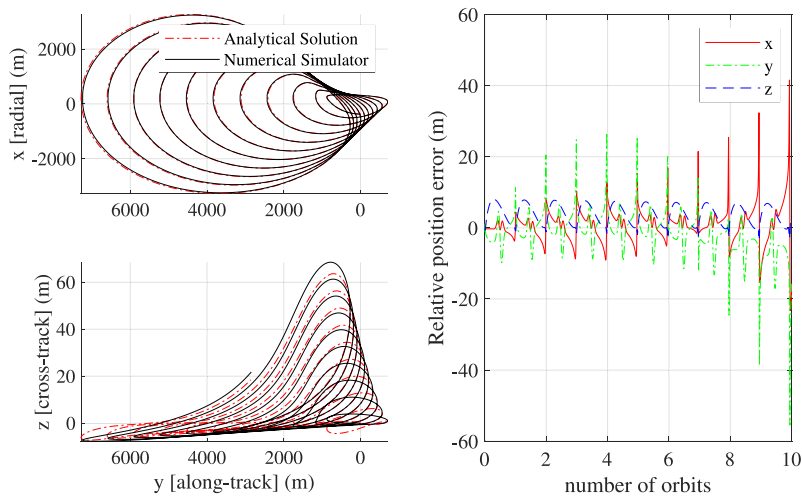


Fig. 17.  $e_c = e_t + 0.00001$ .

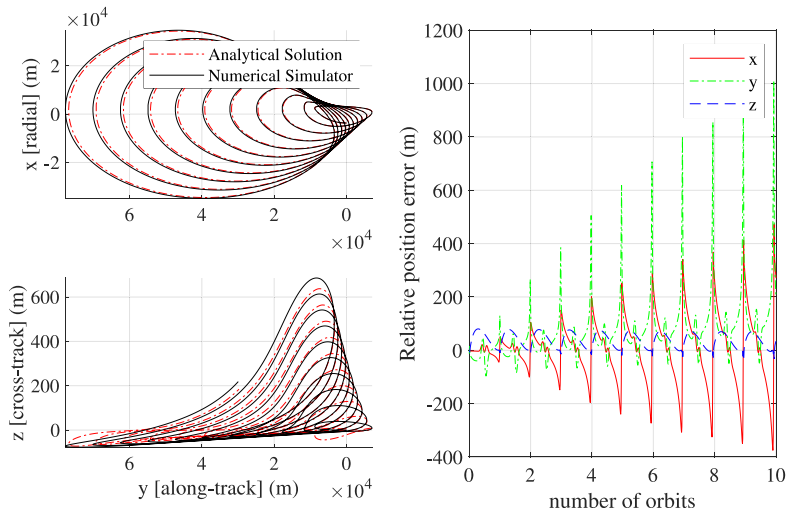


Fig. 18.  $e_c = e_t + 0.0001$ .

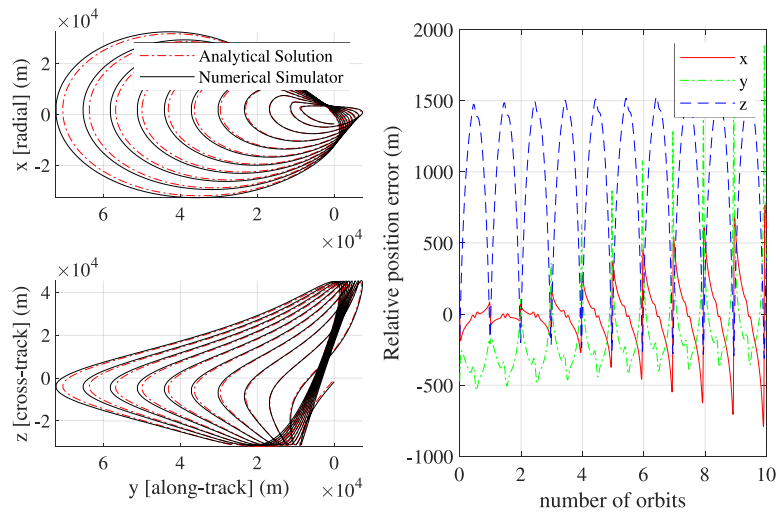


Fig. 19.  $e_c = e_t + 0.0001$  &  $i_c = i_t + 0.1^\circ$ .

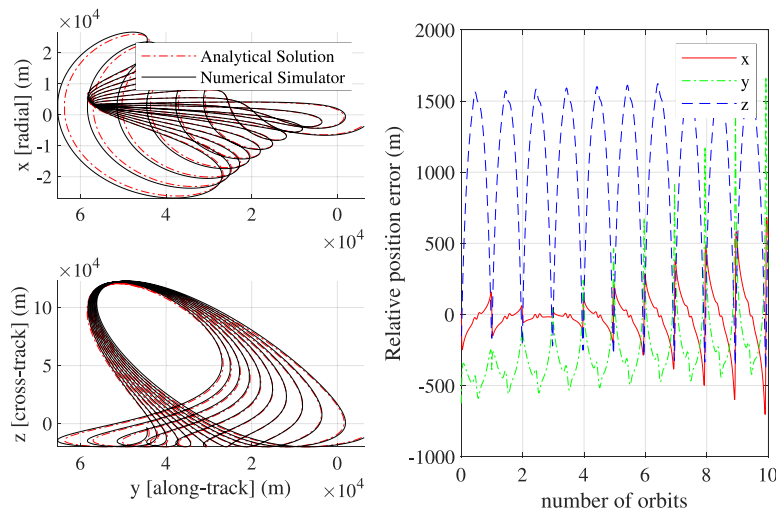


Fig. 20.  $a_c = a_t - 0.01$  km,  $e_c = e_t + 0.0001$ ,  $i_c = i_t + 0.1^\circ$ ,  $\omega_c = \omega_t + 0.1^\circ$ ,  $\Omega_c = \Omega_t - 0.1^\circ$ , &  $\theta_c = \theta_t - 0.1^\circ$ .

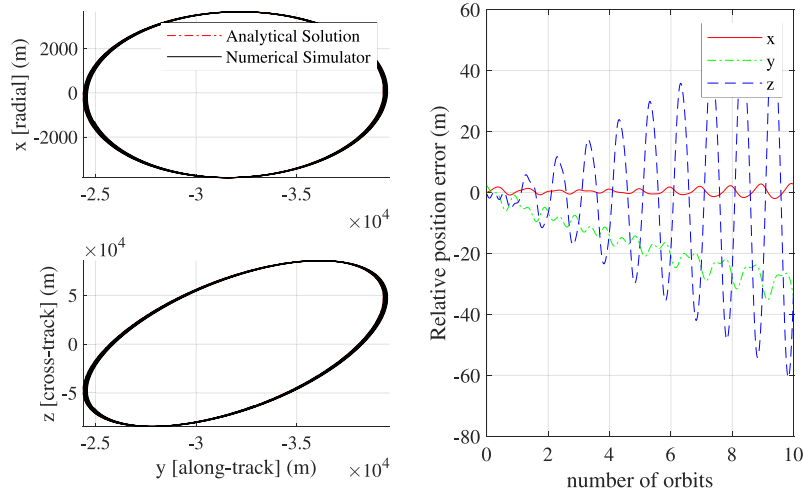


Fig. 21.  $e_t = 0.01$ .

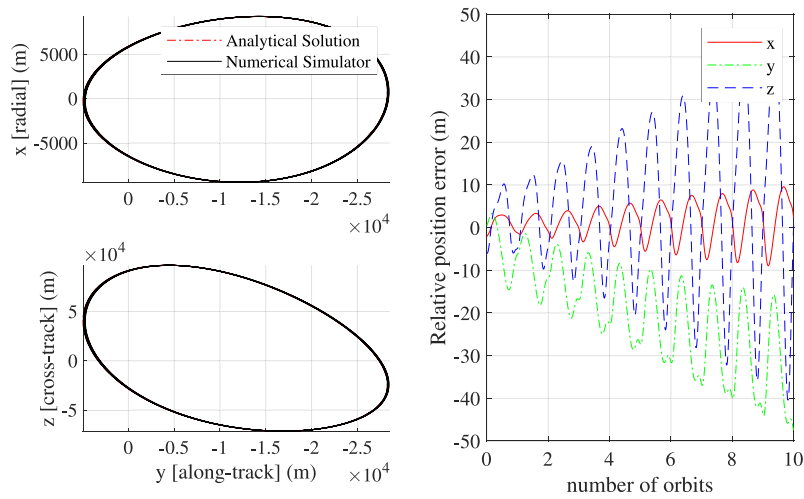


Fig. 22.  $e_t = 0.2$ .

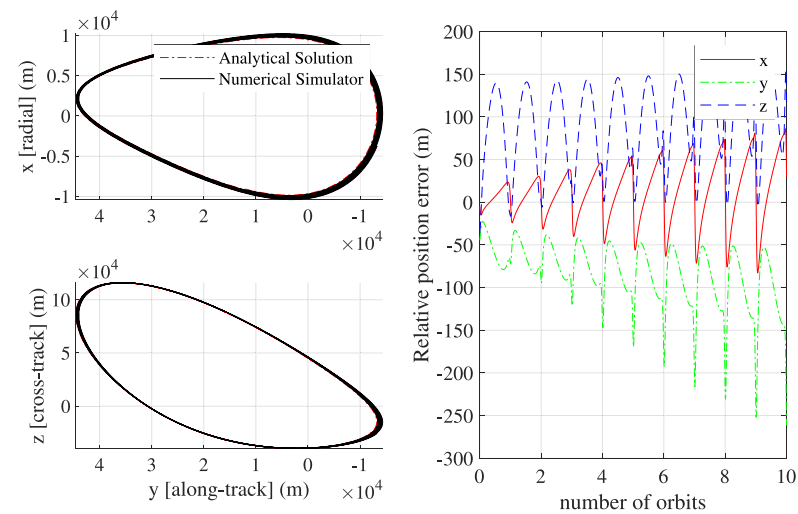


Fig. 23.  $e_t = 0.6$ .

where  $h$  is the orbit angular momentum. As a result, the rate of change of true anomaly undergoes larger variations as eccentricity increases. Hence, the analytical model will result in higher errors since linear approximations of perturbed orbital elements cannot fully capture the effects of the increasing non-linearities between spacecraft's eccentricities and positions on their respective orbits.

## 5. Conclusion

This paper presented a new analytical method for obtaining the relative motion between spacecraft that is applicable to many types of orbits by taking into account perturbations caused by a third body, drag and gravitational field up to the fifth harmonic. Specifically, this paper integrates previously published results that formulated the effects of these perturbations as a function of orbital elements with spacecraft formations, such that an analytical solution that predicts spacecraft relative motion was developed. Previous analysis found in literature addressed the problem of relative motion for long-term analytical propagation; however, the solution presented in this paper was specifically derived for sophisticated guidance and control applications where smaller duration and time-steps are essential in the design. The new method was then validated against a numerical simulator that included effects of gravitational field, third body effects of the sun, moon and solar system planets, ocean and solid Earth tidal effects, relativity and drag. When the analytical solution was compared to the numerical simulator, the relative motion yielded relatively small errors. However, the numerical simulator did not include the effects of solar radiation pressure as part of the ground truth. The solution presented in this paper involved calculating new orbital elements for each spacecraft at every time-step for both the target and the chaser spacecraft which are then used in the non-linear equations of motion to calculate relative motion. Future work will focus on including solar radiation pressure as well as short and long periodic variations due to drag. The accuracy of analytical solution can further be improved by including the inclination, right ascension of the ascending node and argument of perigee of within the third-body model. Furthermore, state-transition matrices based on the newly-developed equations of relative motion will be sought for guidance and control design purposes.

## Declaration of competing interest

The authors declare that they have no known competing financial interests or personal relationships that could have appeared to influence the work reported in this paper.

## References

- [1] S. Curtis, The magnetospheric multiscale mission... Resolving fundamental processes in space plasmas, in: Report of the NASA Science and Technology Definition Team for the MMS Mission, 2005.
- [2] T.V. Peters, J. Branco, D. Escorial, L.T. Castellani, A. Cropp, Mission analysis for PROBA-3 nominal operations, *Acta Astronaut.* 102 (2014) 296–310, <http://dx.doi.org/10.1016/j.actaastro.2014.01.010>.
- [3] W.H. Clohessy, R.S. Wiltshire, Terminal guidance system for satellite rendezvous, *J. Aerosp. Sci.* 27 (9) (1960) 653–658, <http://dx.doi.org/10.2514/8.8704>.
- [4] G. Inalhan, M. Tillerson, J. How, Relative dynamics and control of spacecraft formations in eccentric orbits, *J. Guid. Control Dyn.* 25 (1) (2002) 48–59, <http://dx.doi.org/10.2514/2.4874>.
- [5] G. Hill, *Researches in the lunar theory*, *Amer. J. Math.* 1 (1878) 5–26.
- [6] P. Gurfil, K.V. Kholoshevnikov, Manifolds and metrics in the relative spacecraft motion problem, *J. Guid. Control Dyn.* 29 (4) (2006) 1004–1010, <http://dx.doi.org/10.2514/1.15531>.

- [7] P. Gurfil, K.V. Kholoshevnikov, Distances on the relative spacecraft motion manifold, aiaa guidance, navigation and control conference and exhibit, 2005.
- [8] P. Gurfil, N.J. Kasdin, Nonlinear modeling of spacecraft relative motion in the configuration space, *J. Guid. Control Dyn.* 27 (1) (2004) 154–157, <http://dx.doi.org/10.2514/1.9343>.
- [9] H. Schaub, Incorporating secular drifts into the orbit element difference description of relative orbit, *Adv. Astronaut. Sci.* 114 (2003) 239–258.
- [10] B. Mahajan, S.R. Vadali, K.T. Alfriend, State-transition matrix for satellite relative motion in the presence of gravitational perturbations, *J. Guid. Control Dyn.* (2019) 1–17, <http://dx.doi.org/10.2514/1.G004133>.
- [11] A.W. Koenig, T. Guffanti, S. D'Amico, New state transition matrices for spacecraft relative motion in perturbed orbits, *J. Guid. Control Dyn.* 40 (7) (2017) 1749–1768, <http://dx.doi.org/10.2514/1.G002409>.
- [12] T. Guffanti, S. D'Amico, M. Lavagna, Long-term analytical propagation of satellite relative motion in perturbed orbits, in: *AAS Spaceflight Mechanics Proceedings*, vol. 160, 2017.
- [13] B. Kuiack, S. Ulrich, Nonlinear analytical equations of relative motion on J2-perturbed eccentric orbits, *AIAA J. Guid. Control. Dyn.* 41 (11) (2017) 2666–2677, <http://dx.doi.org/10.2514/1.G003723>.
- [14] D. Brouwer, Solution of the problem of artificial satellite theory without drag, *Astron. J.* 64 (1274) (1959) 378–396, <http://dx.doi.org/10.1086/107958>.
- [15] A.B.A. Prado, Third-body perturbation in orbits around natural satellites, *J. Guid. Control Dyn.* 26 (1) (2003) 33–40, <http://dx.doi.org/10.1155/2008/763654>.
- [16] R. Domingos, R.V. deMoraes, A.F.B.D.A. Prado, Third-body perturbation in the case of elliptic orbits for the disturbing bodies, *Math. Probl. Eng.* 2008 (2008) <http://dx.doi.org/10.1155/2008/763654>.
- [17] Y. Kozai, A new method to compute lunisolar perturbations in satellite motions, *Smithsonian Astrophys. Obs.* (1973) 1–27.
- [18] Y. Kozai, On the effects of the Sun and Moon upon the motion of a close Earth satellite, *Smithsonian Astrophys. Obs.* (1959, Special Report 22).
- [19] D.F. Lawden, *Theory of satellite orbits in an atmosphere*. D. G. King-Hele. Butterworths, London. 1964. 165 pp. Diagrams. 30s., *J. Royal Aeronaut. Soc.* 68 (645) (1964) 639–640.
- [20] J.F. Liu, Satellite motion about an oblate Earth, *AIAA J.* 12 (11) (1974) 1511–1516, <http://dx.doi.org/10.2514/3.49537>.
- [21] Y. Kozai, The gravitational field of the Earth derived from motions of three satellites, *Astron. J.* 66 (1) (1961) <http://dx.doi.org/10.1086/108349>.
- [22] D. Smith, The perturbation of satellite orbits by extra-terrestrial gravitation, *Planet. Space Sci.* 9 (10) (1962) 659–674, [http://dx.doi.org/10.1016/0032-0633\(62\)90125-3](http://dx.doi.org/10.1016/0032-0633(62)90125-3).
- [23] D. Vallado, *Fundamentals of Astrodynamics and Applications*, second ed., Microcosm Press, El Segundo, CA, 2001, pp. 80–81.
- [24] G. Cook, Luni-solar perturbations of the orbit of an Earth satellite, *Geophys. J.* 6 (3) (1962) 271–291, <http://dx.doi.org/10.1111/j.1365-246X.1962.tb00351.x>.
- [25] W. Kaula, Development of the lunar and solar disturbing functions for a close satellite, *Astron. J.* 67 (1962) 300–303, <http://dx.doi.org/10.1086/108729>.
- [26] G.O. Giacaglia, Lunar perturbations of artificial satellites of the Earth, *Celestial Mech. Dynam. Astronom.* 9 (1972) 239–267.
- [27] P. Musen, A. Bailie, E. Upton, Development of the lunar and solar perturbations in the motion of an artificial satellite, NASA-TN D494, 1961.
- [28] C.W.T. Roscoe, S.R. Vadali, K.T. Alfriend, Third-body perturbation effects on satellite formations, *J. Astronaut. Sci.* 60 (3–4) (2015) 408–433.
- [29] I.G. Izsak, Periodic drag perturbations of artificial satellites, *Astron. J.* 65 (5) (1960) 355–357.
- [30] W.C. Guochang Xu, T.-K. Yeh, Analytic solution of satellite orbit disturbed by atmospheric drag, *Mon. Not. R. Astron. Soc.* 410 (1) (2010) 654–662.
- [31] J. Watson, G.D. Misretta, N.L. Bonavito, *An Analytic Method To Account For Drag In The Vinti Satellite Theory*, Greenbelt, Maryland, 1974, pp. 71–92.
- [32] D.A. Danielson, *Semianalytic Satellite Theory* (Master's thesis), Naval Postgraduate School, Monterey, California, 1995.
- [33] V. Martinusi, L. Dell'Elce, G. Kerschen, First-order analytic propagation of satellites in the exponential atmosphere of an oblate planet, *Celestial Mech. Dynam. Astronom.* 127 (4) (2017) 451–476.
- [34] J.P. Vinti, Zonal harmonic perturbations of an accurate reference orbit of an artificial satellite, *Math. Math. Phys.* 67B (4) (1963).
- [35] J.-F. Hamel, J.D. Lafontaine, Linearized dynamics of formation flying spacecraft on a J2-perturbed elliptical orbit, *J. Guid. Control Dyn.* 30 (6) (2007) 1649–1658.
- [36] G. Petit, B. Luzum, IERS Conventions, Technical Report, Frankfurt am Main: Verlag des Bundesamts für Kartographie und Geodäsie, 2010.